XVI International Mineral Processing and Recycling Conference
28-30 May 2025, Belgrade, Serbia

DOI: 10.5937/IMPRC25407K Original research article

METAL RECOVERY FROM SPENT BATTERIES THROUGH ANTISOLVENT CRYSTALLIZATION IN A T-MIXER USING A COUPLED CFD-PBE APPROACH

Vandana Kumari Jha[#], 0000-0003-4013-8218,
Christophe Duwig, 0000-0001-5886-415X,
Samaneh Teimouri, 0000-0003-2511-8040,
Kerstin Forsberg, 0000-0002-3239-5188,
KTH Royal Institute of Technology, Stockholm, Sweden

ABSTRACT – The growing demand for electric vehicles and energy storage systems has led to a rise in battery production, resulting in a growing volume of spent batteries. To address the environmental and economic challenges associated with battery waste, efficient and sustainable recycling processes are crucial. In this context, crystallization offers a promising approach for recovering valuable metals. This study presents a population balance model (PBM) coupled with computational fluid dynamics (CFD) to simulate recovery of nickel sulphate hexahydrate ($NiSO_4 \cdot 6H_2O$) crystals through the antisolvent crystallization technique. Growth and particle size distribution (PSD) of crystals are analyzed within a continuous 3D T-mixer system under laminar flow conditions for a single case of *Re* = 150. The impact of impinging flow on mixing, which affects local supersaturation and PSD, is clearly visible. Additionally, the crystal size at the distribution maximum correlates directly with supersaturation consumption. This approach provides a comprehensive framework for understanding and predicting the PSD in the crystallization process, helping to understand mixing, flow dynamics and supersaturation profiles. This study also evaluates the T-mixer's ability in promoting uniform crystal growth, targeting a narrow PSD. These findings contribute to the development of sustainable crystallization systems, supporting efficient metal recovery in battery recycling applications.

Keywords: Battery Recycling, Population Balance Model (PBM), Antisolvent Crystallization, Metal Recovery, Particle Size Distribution (PSD).

INTRODUCTION

The transition to sustainable energy solutions has become a key priority, as the world moves towards a greener future. Lithium-ion batteries (LIBs) have emerged as a favourable means to attain this goal, offering a promising solution. With their ability to store large amounts of energy in a lightweight and compact form, they have transformed industries ranging from consumer electronics to electric vehicles (EVs). However, LIBs pose significant recycling challenges due to scarcity and valuable constituent metals, such as Ni, Co, Mn [1]. Recycling of cathodes using advanced techniques is essential [2] as they are crucial in terms of cost and effectiveness. This not only supports circular economy [3] but also aligns with Sustainable Development Goals (SDGs) 9 and 12, which

[#] corresponding author: vkjha@kth.se

promote resource efficiency, industry innovation, and waste reduction through recycling [4,5].

Crystallization is a promising method for recovering valuable metals from spent batteries, with particle size distribution (PSD) playing a crucial role in product quality. In antisolvent crystallization, mixing influences nucleation and growth by affecting local supersaturation. High supersaturation can lead to impurity incorporation, while controlled antisolvent addition improves purity [6,7]. Overcoming mixing inefficiencies in traditional batch systems is essential for improving crystal quality and optimizing battery recycling processes [8].

In this study, the population balance model (PBM), coupled with the computational fluid dynamics (CFD), is applied to simulate the evolution of PSD in a continuous 3D T-mixer. The model investigates the influence of reactor hydrodynamics on $NiSO_4 \cdot 6H_2O$ crystallization via the antisolvent method, focusing on flow characteristics, supersaturation profiles, and PSD at *Re* = 150. By understanding the mixing features, influenced by impinging flow, this research aims to enhance crystallization processes for improved product quality, and reduced energy consumption, in battery recycling.

NUMERICAL MODELING

CFD model

CFD is used to s equations governing the balance of momentum, mass, and chemical species. Numerical study is conducted using the commercial CFD software COMSOL Multiphysics® 6.2. The velocity field is solved using the laminar flow interface under steady-state conditions. Simultaneously, the crystallization process is simulated through the chemistry interface, coupled with the transport of concentrated species.

PBM model

Population balance equation (PBE) describes the distribution of characteristic crystal length, represented by the particle diameter. The general form of PBE (Eq. (1)) is expressed as follows [9,10]:

$$\frac{\partial n}{\partial t} + \nabla \cdot (un) + \frac{\partial \left(G(S,L)n(L)\right)}{\partial L} = \nabla \cdot (D \nabla n) + B_{nuc}\delta(L - L_0) + B_{agg} - D_{agg} + B_{break} - D_{break} \quad (1)$$

where n is the number density function (1/m^4), u is the flow velocity (m/s), t is the time (s), $G\ (S,\ L)$ is the size independent particle growth rate (m/s) and is a function of supersaturation, L is the characteristic crystal size (m), D is the diffusion coefficient (m^2/s), B_{nuc} is the nucleation rate (1/(m^4-s), and B_{agg}, B_{break} and D_{agg}, D_{break} represent the birth and death terms (1/(m^4-s) due to agglomeration and breakage, respectively. To solve the discretized PBM in time and space, it needs to be coupled with CFD. For the system considered here, nucleation, agglomeration and breakage terms are neglected.

Supersaturation and crystal growth

Supersaturation is generated by the reduction in solubility caused due to the addition of ethanol in the $NiSO_4 \cdot 6H_2O$-water solution. The initial aqueous nickel sulphate solution

is saturated and contains seeds of $NiSO_4 \cdot 6H_2O$. The size independent growth rate is applied during the crystallization process and is given by the power law kinetics expression as shown in Eq. (2).

$$G = k_g (S-1)^g \tag{2}$$

where S is the supersaturation, k_g is the growth rate constant (m/s), and g the growth rate exponent. The degree of supersaturation in the process is given by:

$$S = \frac{c}{c^*} \tag{3}$$

where c is the concentration of $NiSO_4 \cdot 6H_2O$ and c^* is the equilibrium concentration.

Geometry and meshing

The schematic of the 3D circular T-mixer system is shown in Figure 1(a), illustrating the boundary conditions and dimensions. The computational domain comprises of a T-mixer with two oppositely placed inlets, an outlet and a mixing channel length. One inlet serves for the $NiSO_4 \cdot 6H_2O$-water solution and the other for the ethanol. The study considers a *Re* of 150, which falls within the laminar flow regime. The mean channel velocity is 0.23 m/s and is assumed to be fully developed at the inlets. The system is maintained at a constant temperature of 25°C. A mesh-refinement study was performed, and a custom mesh setting was adopted, as shown in Figure 1(b).

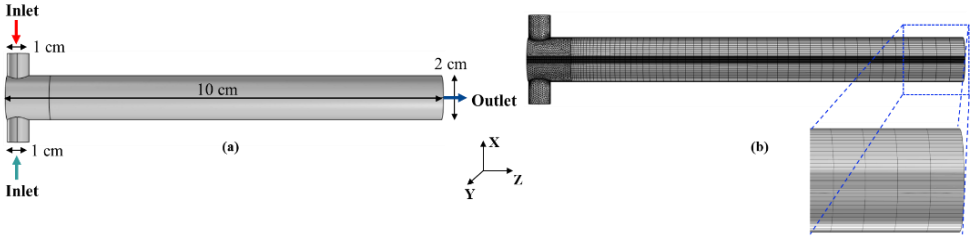

Figure 1 (a) Schematic of the 3D T-mixer geometry; **(b)** depiction of custom mesh

Governing equations and boundary conditions

To simplify the computational model, the following assumptions were made: (a) fully developed flow at the inlets; (b) fluids are incompressible, and density is computed dynamically based on water-ethanol composition; and (c) nucleation, aggregation, and breakage terms were neglected. The governing equations are:

Continuity equation:

$$\nabla \cdot (\rho u) = 0 \tag{4}$$

Incompressible Navier-Stokes equations:

$$\frac{d(\rho u)}{dt} + (\nabla \cdot \rho u u) = -\nabla P + \nabla \cdot \left[\mu \left(\nabla u + (\nabla u)^T \right) \right] \tag{5}$$

where ρ is mixture-density, u is the velocity vector, P is the pressure and μ is the dynamic viscosity.

Transport of species:

$$\frac{d(\rho c)}{dt} + \nabla \cdot (\rho u c) = \nabla \cdot (\rho D \nabla c) + R \tag{6}$$

where *c* is the concentration of the species, *D* is the diffusion coefficient (m^2/s) and *R* is the source term (mol/m3-s). Convective transport was modeled based on the velocity field, while diffusive transport was modeled according to Fick's law.
Boundary conditions: Fully developed flow is applied at the respective fluid inlets and no-slip boundary conditions at the walls. A Dirichlet boundary condition was defined at each inlet setting the ingoing number density for each interval to zero, except for interval 1 at inlet 1. Additional details are provided in Table 1.

Table 1 Summary of boundary conditions

Condition	Equation	Applied at
Constant velocity	$v = v_A$	Inlet 1
Constant velocity	$v = v_O$	Inlet 2
No-slip	$v = 0$	T-mixer walls
Pressure outlet	$P = P_{atm}$	Outlet
$NiSO_4.6H_2O$ concentration	$c_{NiSO4.6H2O} = c_{inlet,NiSO4.6H2O}$	Inlet 1
C_2H_5OH concentration	$c_{C2H5OH} = c_{inlet,C2H5OH}$	Inlet 2
Outflow	$\frac{\partial c}{\partial n} = 0$	Outlet

RESULTS AND DISCUSSION

Flow characteristics

The flow characteristics of the mixing channel at *Re* = 150 is illustrated in Figure 2(a)-(b), highlighting velocity contours at different cross-sections, and streamlines in both 3D and 2D views. The velocity distributions at multiple cross-sections along the main mixing channel, showing how flow evolves downstream, is displayed. The enlarged inset provides a detailed view of velocity variations at a specific cross-section, revealing regions of high and low flow intensity. The streamlines depicting fluid motion, with a zoomed-in view near the inlet showing strong mixing and recirculation zones, are also presented in a 2D view. High velocity regions are seen near the inlet and lower velocities further downstream. As the flow progresses, it becomes more homogeneous along the length of the channel. The geometry features a mixing channel significantly longer than the mixing zone, ensuring sufficient residence time. This visualization helps analyze mixing efficiency and hydrodynamic effects, crucial for crystallization process.

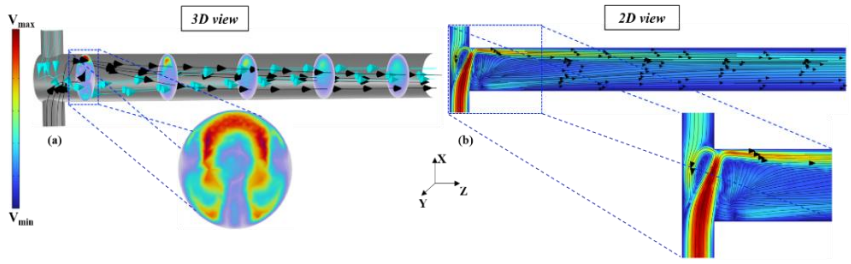

Figure 2 Contour and streamline plots shown at a center cut XZ-plane inside the T-mixer along with the insets, at Re = 150: (a) in 3D view; (b) 2D view

Supersaturation profiles

The supersaturation plot along the centerline of the T-mixer channel geometry is shown in Figure 3, illustrating how mixing influences the spatial variation of supersaturation. The supersaturation is more evenly distributed along the channel length, promoting uniform crystal growth and resulting in a narrower outlet size distribution. The left side corresponds to the inlet region, where the antisolvent and solution first interact, generating a high supersaturation zone. As the flow progresses downstream, supersaturation decreases due to mixing and diffusion, and crystal formation, indicating lower supersaturation levels. The smooth gradient suggests a gradual mixing process. Understanding this distribution is crucial for optimizing crystal growth and ensuring uniform particle size.

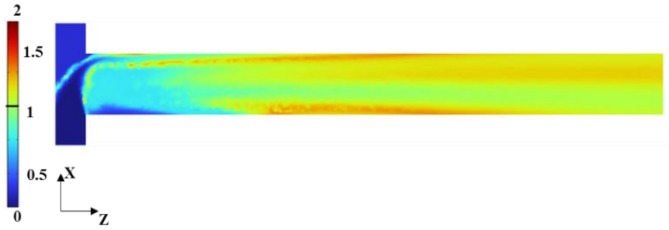

Figure 3 Supersaturation plot shown at a center cut XZ-plane inside the T-mixer

Particle size distribution

Particle size analysis was done at the XZ- and XY-planes, as shown by different cut planes (Figure 4(a)). The spatial evolution of crystal size along the length of the channel is shown in Figure 4(b). There is an increase in crystal size as the seeds flow from inlet to the outlet, suggesting crystal growth with the increase in residence time. Normalized number density at: outlet (Z = 0 cm), Z = 2.5 cm and Z = 5 cm is shown (Figure 4(c)). The distribution shows a shift in the particle size towards larger values as the particles approach the outlet, i.e., as the value of Z decreases. This trend confirms the progressive growth of crystals along the flow direction, and peak around 10-11 µm, indicating most crystals form within this range. Gradual broadening of peaks suggests a wider distribution, due to the effects of hydrodynamics and local supersaturation.

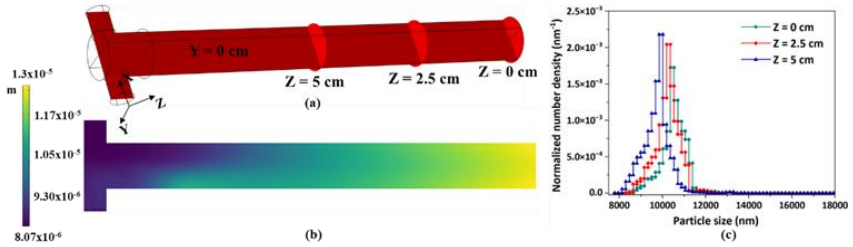

Figure 4 (a) Different cut planes shown inside the T-mixer; (b) contour plot showing the distribution of crystal size at XZ-plane where Y = 0; (b) normalized distribution at the outlet (Z = 0 cm), Z = 2.5 cm and Z = 5 cm

CONCLUSION

This study presents a comprehensive numerical approach integrating CFD with the PBM to simulate the antisolvent crystallization of nickel sulphate in a continuous 3D T-mixer geometry. The model accurately predicts the particle size distribution (PSD) under steady-state laminar flow conditions (*Re* = 150). The numerical results provide insights into the influence of flow dynamics and mixing intensity on crystal growth and PSD. The impact of impinging flow on local supersaturation levels is also highlighted, emphasizing its role in crystallization efficiency. Additionally, this study evaluates the T-mixer's ability to promote uniform crystal growth, targeting a narrow PSD, high-purity crystals, and improved recovery rates. These findings contribute to the development of sustainable crystallization systems, supporting efficient metal recovery in battery recycling applications.

ACKNOWLEDGEMENT

The simulations and data management were performed using the resources provided by the National Academic Infrastructure for Supercomputing in Sweden (NAISS) at the PDC Center for High Performance Computing, partially funded by the Swedish Research Council, Sweden through grant agreement no. 2022-06725. The authors are grateful to the Swedish Energy Agency, Sweden for funding this research work within the program Batterifonden.

REFERENCES

1. I. Energy Agency, Global EV Outlook 2022 (2022) Securing supplies for an electric future. www.iea.org/t&c/.
2. Fraser, J., Anderson, J., Lazuen, J., Lü, Y., Heathman, O., Brewster, N., Bedder, J., Masson, O. (2021) Study on future demand and supply security of nickel for electric vehicle batteries. Publications Office of the European Union.
3. Geissdoerfer, M., Savaget, P., Bocken, N.M.P., Hultink, E.J. (2017) The Circular Economy – A new sustainability paradigm?. J Clean Prod, 143, 757–768.
4. Department of Economic and Social Affairs. Goal 9. eng. year missing. url:sdgs.un.org/goals/goal9 (visited on 23/01/2025).
5. Department of Economic and Social Affairs. Goal 12. eng. year missing. url:sdgs.un.org/goals/goal12 (visited on 23/01/2025).
6. Moldoveanu, G.A., Demopoulos, G.P. Producing (2002) High-Grade Nickel Sulfate with Solvent Displacement Crystallization. J. Met., 49–53.
7. McGinty, J., Chong, M.W.S., Manson, A., Brown, C.J., Nordon, A., Sefcik, J. (2020) Effect of process conditions on particle size and shape in continuous antisolvent crystallisation of lovastatin. Crystals (Basel), 10, 1–17.
8. Madane, K., Ranade, V.V. (2022) Anti-solvent crystallization: Particle size distribution with different devices. Chemical Engineering Journal, 446, 137235.
9. Schwarzer, H.C., Peukert, W. (2004) Combined experimental/numerical study on the precipitation of nanoparticles. AIChE Journal, 50, 3234–3247.
10. Tang, H.Y., Rigopoulos, S., Papadakis, G. (2022) On the interaction of turbulence with nucleation and growth in reaction crystallisation, J Fluid Mech, 944.